Hybrid x-ray/optical luminescence imaging: Characterization of experimental conditions

C. M. Carpenter,[a] C. Sun, and G. Pratx
Department of Radiation Oncology, School of Medicine, Stanford University, Stanford, California 94305

R. Rao
SRI International, Menlo Park, California 94025

L. Xing
Department of Radiation Oncology, School of Medicine, Stanford University, Stanford, California 94305

(Received 21 April 2010; revised 28 May 2010; accepted for publication 6 June 2010; published 13 July 2010)

Purpose: The feasibility of x-ray luminescence imaging is investigated using a dual-modality imaging system that merges x-ray and optical imaging. This modality utilizes x-ray activated nanophosphors that luminesce when excited by ionizing photons. By doping phosphors with lanthanides, which emit light in the visible and near infrared range, the luminescence is suitable for biological applications. This study examines practical aspects of this new modality including phosphor concentration, light emission linearity, detector damage, and spectral emission characteristics. Finally, the contrast produced by these phosphors is compared to that of x-ray fluoroscopy.
Methods: Gadolinium and lanthanum oxysulfide phosphors doped with terbium (green emission) or europium (red emission) were studied. The light emission was imaged in a clinical x-ray scanner with a cooled CCD camera and a spectrophotometer; dose measurements were determined with a calibrated dosimeter. Using these properties, in addition to luminescence efficiency values found in the literature for a similar phosphor, minimum concentration calculations are performed. Finally, a 2.5 cm agar phantom with a 1 cm diameter cylindrical phosphor-filled inclusion (diluted at 10 mg/ml) is imaged to compare x-ray luminescence contrast with x-ray fluoroscopic contrast at a superficial location.
Results: Dose to the CCD camera in the chosen imaging geometry was measured at less than 0.02 cGy/s. Emitted light was found to be linear with dose ($R^2=1$) and concentration ($R^2=1$). Emission peaks for clinical x-ray energies are less than 3 nm full width at half maximum, as expected from lanthanide dopants. The minimum practical concentration necessary to detect luminescent phosphors is dependent on dose; it is estimated that subpicomolar concentrations are detectable at the surface of the tissue with typical mammographic doses, with the minimum detectable concentration increasing with depth and decreasing with dose. In a reflection geometry, x-ray luminescence had nearly a 430-fold greater contrast to background than x-ray fluoroscopy.
Conclusions: X-ray luminescence has the potential to be a promising new modality for enabling molecular imaging within x-ray scanners. Although much work needs to be done to ensure biocompatibility of x-ray exciting phosphors, the benefits of this modality, highlighted in this work, encourage further study.
[DOI: 10.1118/1.3457332]

Key words: molecular imaging, x-ray, optical, luminescence

I. INTRODUCTION

Molecular imaging promises increased sensitivity and specificity to disease compared to traditional anatomical imaging modalities. The information gained from molecular imaging has the potential to provide patient-specific selection of therapy, improved prediction of outcomes, and increased treatment efficacy.[1] X-ray radiography and computed tomography (CT) are commonly used anatomical imaging modalities; however, although they provide invaluable information in the clinic, they have been largely unsuccessful for molecular imaging.[2] This deficiency is due to their lack of sensitivity to low concentrations of contrast agents; x-ray imaging is many orders of magnitude less sensitive than optical[3] or radionuclide[4] imaging. This poor sensitivity arises from the low x-ray stopping power of diluted contrast agents, which necessitates high concentrations compared to other imaging modalities.[2]

Phosphors are well-established materials used universally in cathode ray tubes and light-emitting diodes for their ability to emit light upon excitation by electrons or photons. Phosphors are solid-state crystals, and can be doped with transition metals or lanthanide ions. These materials form a system optimized to capture higher-energy radiation and emit downconverted energy as optical photons. In the context of an x-ray scanner, x-ray photons transfer some or all of their energy to electrons in the solid-state crystal through Comp-

ton and photoelectric interactions.[5] These high-energy electrons progressively lose energy through interactions with the atoms, leaving a track of excited electrons behind. When the energy of the excited electrons in the conduction band is reduced to approximately two to three times the band gap of the dopant, they may migrate into the luminescence center of the phosphor, and recombine with holes to emit light.[6] Thus, this amplification process results in effective emission efficiencies (photons emitted divided by the photons absorbed), which can be much greater than 1. For example, on average, 6000 photons are produced for each 100 keV x-ray photon absorbed in one particular gadolinium oxysulfide:terbium phosphor.[7] The emitted light may then be imaged by sensitive optical detectors.

This paper investigates the use of nanosized inorganic phosphors[7] as potential biological contrast agents for medical imaging in a combined x-ray/optical instrument. The emission from this contrast agent is evaluated to determine the practicality of this new modality. The implications for this x-ray activated contrast agent are discussed with regard to its potential to enable molecular imaging during fluoroscopy, x-ray CT, or projection x-ray imaging.

II. METHODS

II.A. Phosphor fabrication

Trivalent europium (Eu) or terbium (Tb) activated gadolinium oxysulfides (GOS) or lanthanum oxysulfides (LOS) were synthesized using appropriate rare earth nitrates (99.99% pure) with two standard methods: The gel-polymer combustion process and the combination capping process,[6] respectively. After preparation, samples were heat treated at 500–600 °C for 1–3 h to aid the migration of the dopant into the crystal lattice structures. Next, the powders were ball milled with glass beads (10 μm) in the presence of the appropriate surfactant for 2–3 h.

II.B. Spectroscopy and imaging of phosphor characteristics

To facilitate spectroscopy and imaging for the analysis of the properties of the phosphors, dry phosphor was placed in plastic test tubes. For spectroscopy, the distal end of a 10 m, 400 μm optical fiber was placed in contact with the side of the test tube, while the proximal end was attached to a spectrophotometer (Jaz, Ocean Optics, Dunedin, FL), which was operated from the x-ray control room. Optical emission spectra across the visible and near infrared (NIR) range were acquired with the SPECTRASUITE (Ocean Optics) software package. Imaging was performed with a 512×512 pixel backilluminated CCD camera (CCD temperature maintained at −70 °C) with a F1.4 imaging lens, exposure times varying from <1 to 60 s, and the lens aperture fully open. During data acquisition, the imaging camera was shielded with lead bricks and placed 15–20 cm outside the direct field of radiation to protect from ionizing radiation. The optics setup was placed inside a light-tight box to eliminate ambient room light. A schematic of this imaging setup is shown in Fig. 1(a), and a photograph of the setup during experimental imaging is shown in Fig. 1(b).

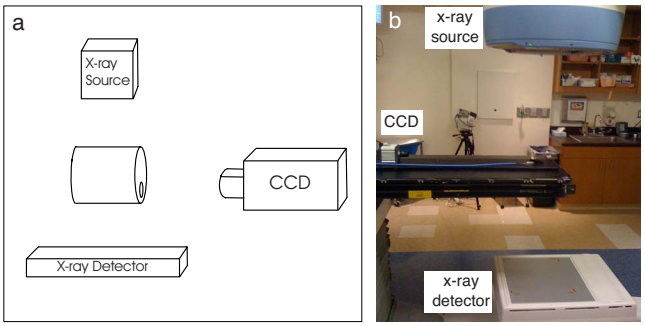

FIG. 1. (a) Schematic of the experimental setup including the CCD camera, the x-ray source and detector, and the sample. (b) Photograph of the imaging setup.

A cone beam computed tomography (CBCT) system (Acuity, Varian Medical Systems, Palo Alto, CA) was used to irradiate the sample. This system allows both CBCT and fluoroscopy at various tube voltages between 70 and 125 kV. This system was operated in fluoroscopy mode to enable continuous irradiation from a constant geometry.

II.C. Concentration evaluation

Minimum detectable concentrations were calculated, assuming a superficial location of the phosphor contrast agent (i.e., no signal loss due to tissue absorption). Including light detection losses L, the light detected Φ is

$$\Phi = \Gamma \cdot D \cdot c \cdot L, \tag{1}$$

where Γ is the effective emission efficiency, D is the dose, and c is the concentration of the phosphor. From Ref. 8, the effective emission efficiency (in a lanthanum oxysulfide:terbium phosphor) is 1.39×10^{15} optical photons/(Gy mg). We assumed 99% detection loss due to suboptimal optical collection geometry. Signal below a signal-to-noise ratio (SNR) of 10 (assuming shot-noise limited detection) was assumed to be too low to detect. To calculate the molar concentration, we assumed a spherical 10 nm diameter nanoparticle consisting of hexagonal-structured phosphors with lattice constants of $a=4.046$ Å and $c=6.951$ Å (Ref. 9) and density of 5.5 g/cm^3.[10]

II.D. Optical phantom fabrication and imaging

A small-animal sized tissue-simulating phantom was fabricated for this study. The cylindrical phantom measured 2.5 cm in diameter×4.5 cm in height, with a 1 cm × 2.5 cm cylindrical inclusion. The phantom was made from 1% agar with homogeneous optical properties using titanium oxide for scatter and India Ink for absorption using methods common to diffuse optical phantoms.[11] The optical properties were determined by a previously established system[12] to be $\mu_a=0.0025$ mm^{-1} and $\mu_s'=0.77$ mm^{-1} at 630 nm. Micrometer-sized GOS:Eu phosphor particles were added to the inclusion at a concentration of 10 mg/ml, and no phosphor was added to the background. This phantom was

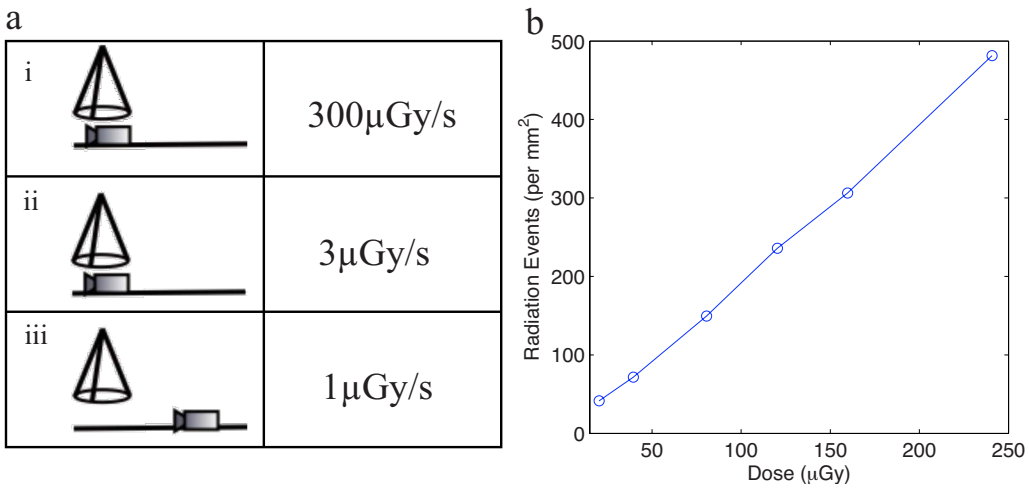

FIG. 2. (a) Radiation dose on the detector for three different configurations: (i) Direct irradiation, (ii) direct irradiation with lead shielding (5 mm on top, 50 mm on each side), and (iii) indirect irradiation with lead shielding. (b) Radiation events per area per dose.

imaged with an electron multiplied (EM)-CCD (Hamamatsu ImageEM 9100-13, Hamamatsu, Japan) with a 512 $\times$512 pixel sensor cooled at −70 °C, with a F1.4 imaging lens, with exposure of times less of 2 s, gain at half-maximum, and the lens aperture fully open.

III. RESULTS

III.A. CCD interaction with ionizing radiation

To ensure that the CCD camera would not be damaged from the ionizing radiation, an ionization chamber (PTW Farmer 30010, PTW Freiberg GMBH, Germany) was placed in the radiation field to determine the dose to air in the vicinity of the CCD. Several locations along the patient bed were measured to determine dose rate, as indicated in Fig. 2(a). Under direct radiation, the dose was nearly 300 μGy/s; this dose rate was reduced by two orders of magnitude by placing lead around the chamber, and further by twofold, to 1.5 μGy/s, by moving the chamber 15 cm out of the radiation field. This rate deposits dose well below levels that would likely damage the CCD.

To investigate camera damage further, we investigated the lingering effects of radiation on the CCD. The interaction of an x-ray photon with the CCD camera appears in the image as a bright pixel at near-maximum intensity. These hot pixels appear similar to cosmic ray interactions, which are common with CCD cameras. We investigated the incidence of these events for a typical setup using a CCD to radiation field distance of 15 cm and 6 mm of lead shielding above the camera to protect from x-ray collimator leakage. Radiation events were determined by performing an intensity threshold on an image acquired with the lens cap on. It is clear from Fig. 2(b) that the number of radiation events is linear with dose, and thus there were no lingering effects from the radiation. To improve image quality, denoising strategies may be employed utilizing this linearity, such as an automatic selection of a hot-pixel threshold, which is dependent on camera dose. Further consideration of the damage limits of CCD cameras is given in Sec. IV.

III.B. Phosphor characterization

III.B.1. Spectral emission

A large body of knowledge exists on phosphors due to over a half-century of study of optimizing phosphors for such applications as light-emitting diodes, cathode ray tubes, and scintillators for medical imaging. This work has resulted in a library of crystals and dopants from which one may select an emission wavelength that is ideal for a particular application.[6] We investigated the feasibility of GOS phosphors, which were doped with either terbium (GOS:Tb) or europium (GOS:Eu), because of their absorption K-edge in the diagnostic energy regime at approximately 50 keV.[13] Figure 3(a) shows the emission of these phosphors under 100 kV x-ray irradiation. The GOS:Tb phosphor had a maximum peak emission of 545 nm in green, whereas the GOS:Eu phosphor had several peaks of longer wavelengths in the NIR, including 596, 618, 627, and 707 nm, with an emission maximum at 627 nm. The flexibility enabled by modifying the dopant is of great value for matching the emission wavelength to a particular application, such as the absorption peak of a phototherapeutic drug,[14] or the tissue absorption minimum for optical imaging in deep tissue.[15]

III.B.2. Light output vs dose

To determine the linearity of light output from phosphor, GOS:Tb was dispersed in a cuvette containing 1% agar at a concentration of 10 mg/ml. The phosphor solution was placed at the same source-target distance as the ionization chamber. The x-ray system was operated in fluoroscopy mode and the tube voltage was set to 100kV. The dose was linearly increased by two methods. First, the tube current was increased from 5 to 20 mA with a constant tube voltage.

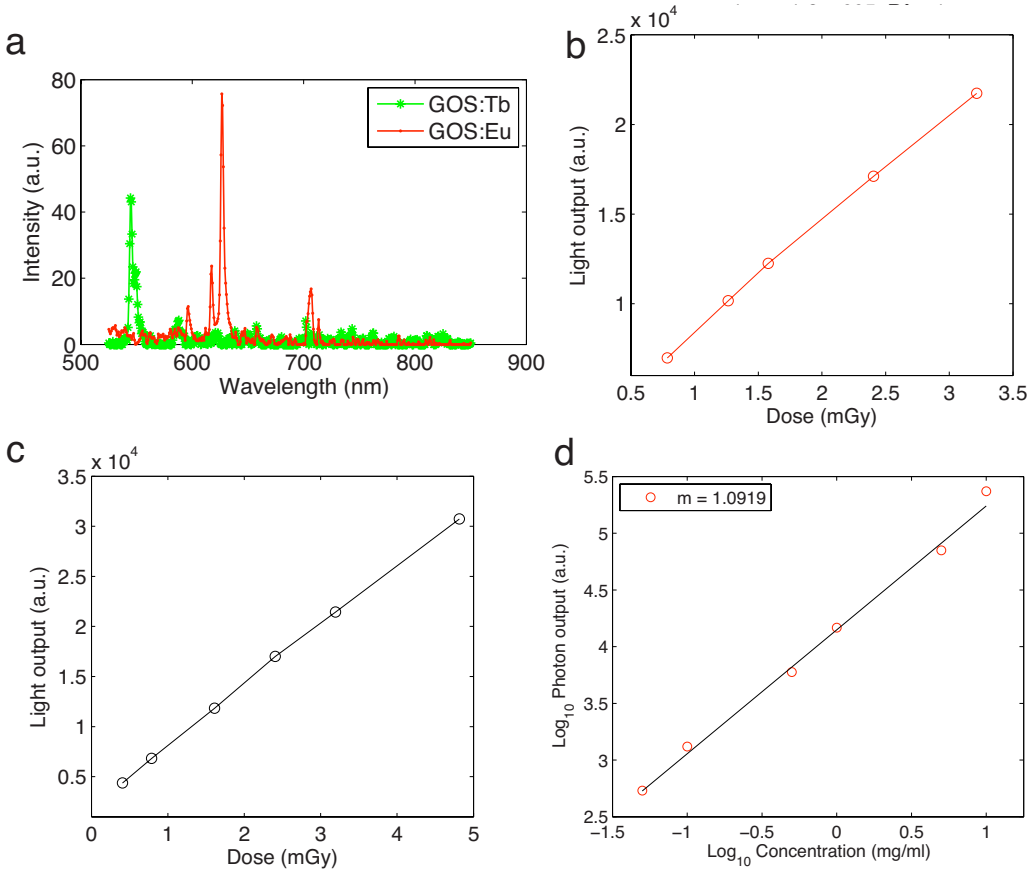

FIG. 3. (a) Emission spectra of GOS phosphors under x-ray excitation. GOS:Tb, with an emission peak at 545 nm, is labeled with asterisks (*), and GOS:Eu, with emission peaks at 596, 618, 627, and 707 nm. (b) X-ray induced GOS:Tb Photon output vs dose with dose varied by increasing tube current. (c) Photon output vs dose with dose varied by increasing irradiation time. For both methods, photon output is linear with dose shown in terms of current ($r=1$, $p<0.001$, $R^2=1$). (d) Photon output vs concentration for the GOS:Eu phosphor. Concentrations were measured via microcuvette and dispersed in 1% agar. Photon output is linear with concentration ($r=0.99$, $p=1.9\times10^{-7}$).

Second, the tube voltage and current remained constant, and dose was linearly increased by adjusting the irradiation time. Images were acquired with a CCD camera, with the exposure time optimized. All measurements were denoised for hot spots and identical regions of interest (ROIs) were selected for analysis.

Both current/dose and time/dose linearity were confirmed by running a linear correlation analysis (correlation coefficient of 1.0, $p<0.001$). Figure 3(b) shows the linearity in dose using the first method, which showed significant linearity (correlation coefficient of 1.0, $p<0.001$), while Fig. 3(c) confirms linearity with the second method (correlation coefficient of 1.0, $p<0.001$).

III.B.3. Light output vs concentration

To assess the light output due to various phosphor concentrations, dilutions of GOS:Eu phosphors from 5 μg/ml to 10 mg/ml were dispersed in 1% agar. Cuvettes were placed in a 50 kV, 30 mA x-ray source and imaged with a CCD camera. ROIs were selected to contain similar areas of the cuvettes, and the signal was normalized according to exposure time. Hot spots were removed from the images prior to analysis.

The results shown in Fig. 3(d) demonstrate a strong linearity (linear correlation coefficient of 0.99, $p<0.001$) with a slope of 1.09. The slight departure of the slope from unity is most likely due to errors in selecting identical ROIs for the different cuvettes and may have resulted in the inclusion of the cuvette wall in the ROI, which exhibited some light piping.

III.C. Minimum detectable concentrations

We calculated the minimum detectable concentration according to the methodology outlined in Sec. II C, for doses ranging from 1 cGy (less than the typical mammographic dose) to 20 Gy (a typical dose delivered in single-dose intraoperative radiation therapy). In addition, we calculated the minimum detectable concentration for several phosphor efficiencies, scaled according to that reported by Kandarakis *et al.*[8] (i.e., 100% is equivalent to the efficiency reported). Figure 4 shows the minimum detectable concentrations for these scenarios. According to these calculations, picomolar (ng/ml) concentrations are detectable (SNR of 10) with a LOS phosphor for mammographiclike dose, while therapy doses allow femtomolar (pg/ml) concentrations to be detected.

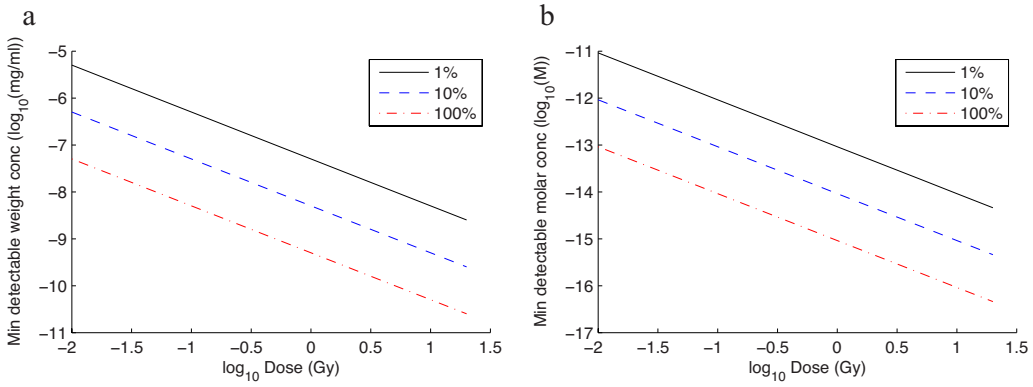

FIG. 4. Minimum estimated phosphor concentrations calculated from the literature and our own data. Lines represent phosphor luminescence efficiencies; the 100% line is based on efficiency data from a $La_2O_2S:Tb$ phosphor reported by Kandarakis *et al.* (a) Minimum weight concentration (in mg/ml) vs dose (Gy). (b) Minimum molar concentration (in M) vs dose (Gy).

III.D. Contrast comparison between x-ray/optical and fluoroscopy

The recovered contrast between an inclusion with phosphor and a background without phosphor was investigated to compare the contrast differences between x-ray fluoroscopy and x-ray/optical luminescence imaging in the small-animal imaging phantom described in Sec. II D. The phantom was imaged during fluoroscopy operation with the tube voltage at 100 kV and the tube current at 10 mA. The x-ray source was placed above the phantom to evenly irradiate the volume. The CCD camera was placed within 15 cm of the phantom and oriented orthogonal to the direction of irradiation. The fluoroscopy image was taken simultaneously. It is important to note that gadolinium is a strong absorber of 100 keV x-ray energy, with a mass attenuation coefficient of 3.109 cm^2/g (compared to common x-ray contrast agents such as barium at 2.196 cm^2/g and iodine at 1.942 cm^2/g). Since gadolinium has a higher mass attenuation coefficient for x-ray photons than water (mass attenuation coefficient of 0.1707 cm^2/g), it should exhibit slight contrast.

The images from the phantom are shown in Fig. 5. Figure 5(a) shows a white light image taken by the CCD camera with background illumination from the room lights. The corresponding fluoroscopy image is shown in Fig. 5(b). The phosphor inclusion is indicated by the arrow and shows slight increased x-ray absorption (the smaller dark circle is a bolt hole in the aluminum optical table). Figure 5(c) shows a raw optical image taken of the x-ray luminescent phosphor. This image is overlaid on the white light image in Fig. 5(d). The contrast between the inclusion and the background is very slight, at 0.6% for the fluoroscopy image, while it is over 260% for the luminescence image. In addition, the signal-to-noise ratio for the phosphor emission was 23 vs 2.4 for the fluoroscopy image.

IV. DISCUSSION

We found that dose distributed to the shielded camera was measured at less than 3 μGy/s when the camera was positioned at the isocenter and the x-ray tube voltage was 100 keV with the tube current at 20 mA. Although this dose is low, estimating a damage threshold is difficult for CCDs because damage is design/manufacturer-specific and is dependent on environmental conditions (for a more thorough overview, see Ref. 16). It is well recognized that the largest radiation threat to the operation of a CCD is the bombardment by highly energetic heavy particles, such as protons and neutrons. These particles contribute most to CCD damage through impact displacements of silicon atoms which create semipermanent energy traps. These traps create energy levels which can increase Johnson noise (via promoting valence band electrons to the conduction band), create spurious noise when trapped electrons are released, and alter the operation of transistor gates by altering their flat-band voltage (for a more thorough review, see Refs. 17 and 18). Although the probability of creating protons and neutrons is extremely low

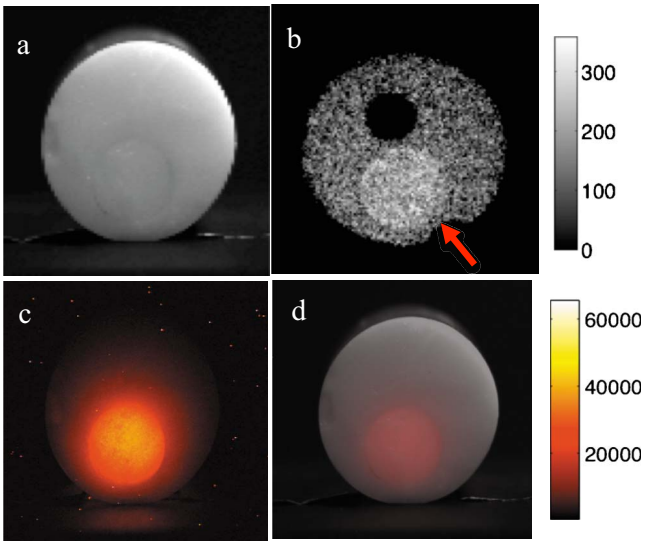

FIG. 5. Agar imaging phantom with embedded phosphors and tissue emulating optical properties. (a) White-light optical image. (b) Projection fluoroscopy image (note the distinction between the phosphor inclusion—indicated by the arrow—around 300 units, compared to the black circle caused by a screw hole in the optical table supporting the phantom). (c) Optical emission from the phantom. (d) Overlay of the white light image (a) and the light emission (c).

at diagnostic x-ray energies studied here, it is relevant for therapeutic energies in the MV range. Cumulative doses are also important because of the increased probability for a high-energy photon interaction. It has been reported that total doses above about 25 and 100 Gy are considered thresholds for increased noise and permanent damage, respectively[19] (though again, these numbers are highly camera-dependent). Thus, it is important to keep radiation dose on the CCD as low as possible to minimize cumulative dose and increase the life of the camera. The dose deposited in this experiment of 1–3 μGy/s is minimal, and damage due to radiation should be insignificant in the lifetime of the camera.

The lanthanide dopants examined in this study are known to have extremely sharp peaks; for example, we measured the full width at half maximum (FWHM) of the GOS:Tb sample at 3 nm, while the GOS:Eu sample had a FWHM of 2 nm for the largest peak [both shown in Fig. 3(a)]. This is in contrast to common fluorophores like indocyanine green, which often have an emission peak FWHM of about 60 nm. This enables the possibility of multiplexing contrast agents with very little cross-talk, allowing the simultaneous measurement of several markers for disease.

A major concern of these x-ray excitable phosphor contrast agents is that they require ionizing dose to activate. Thus, lower concentrations of phosphors will necessitate higher doses. We analyzed the practical detection limit of phosphors using the knowledge of concentration and dose linearity and luminescence efficiencies found in the literature for similar nanophosphors. For detection at the surface of tissue, x-ray mammographic dose should be sufficient to allow the detection of picomolar (ng/ml) concentrations of phosphor. This finding is corroborated with our experimental results shown in Fig. 3. If the data in Fig. 3(d) are extrapolated to 10 counts/pixel, adequate signal-to-noise ratio is achieved using an EM-CCD camera (with dark noise of 0.05 counts/pixel for this acquisition). Placing the camera within a few cm (compared to 20 cm in this experiment) would result in the detection of approximately two orders of magnitude more light. Further, if the dose is increased by an order of magnitude [from the 4 mGy dose administered for Fig. 3(d)] to mammography levels, and EM gain is increased to the maximum, concentrations of ng/ml (picomolar) may be realized.

At deeper depths, however, light attenuates rapidly; for example, in breast tissue, a depth of 3 cm would attenuate detected light by approximately three orders of magnitude.[20] This would effectively decrease phosphor sensitivity during mammographic dose to nanomolar concentrations. In a radiation oncology setting, however, high doses are delivered to treat disease (such as the 20 Gy single-fraction therapy, which is used during intraoperative radiation therapy[21]). This technique could aid a surgeon and radiation oncologist to identify the distribution of disease around a tumor margin, such as during breast lumpectomy. In this case, the patient would be injected with a phosphor contrast agent before or during surgery, depending on the pharmacokinetics of the tracer. The tracer could be imaged during the first 1% or 10% (e.g., 0.2 or 2 Gy) of the radiotherapy treatment dose, which would provide the clinicians with more confidence about the treatment dose or volume, or enable an adjustment to the dose distribution.

The other area of concern with these particles is biological compatibility. This is an issue for all nanoparticle systems, and much work is being done to develop strategies to ensure stability and compatibility.[22] In fact, multiple groups have successfully used upconversion phosphors in small-animal models.[23,24] The increased interest in phosphors should aid in the rapid advancement in biocompatibility, which will aid this modality.

We found that the contrast to background ratio was over 2.5 orders of magnitude higher for optical detection of the luminescent phosphors compared to x-ray fluoroscopy. The actual contrast amplification is much higher since the optical photons emitted from the inclusion exhibit extensive scatter in the background and subsequently are detected by the CCD. These scatter effects would be greatly minimized via modeling of the light propagation. In comparison, x-ray photon scatter is relatively nonexistent so that the signal contribution from the background originating from the inclusion is negligible. Considering the photon scatter should greatly improve the contrast of these phosphors for optical detection compared to fluoroscopy.

Although this work demonstrated the potential of x-ray luminescence imaging for imaging a superficial object, imaging of lesions centimeters deep should be possible, with contrast-resolution limitations dependent on tissue properties, concentration, and nonspecific uptake. The development of deep-tissue x-ray luminescence imaging will require the incorporation of optical tomographic models. With x-ray luminescent imaging, the x-ray source must be modeled in tissue to give an accurate description of dose. There are many sophisticated tools to model dose, such as Monte Carlo or analytical models, which have been shown to be accurate [e.g., within 4% (Ref. 25)] in biological tissues. Concurrent x-ray structural imaging will further improve these calculations. After dose distribution is calculated, tomographic imaging may be performed with a reconstruction model that uses a model of the light propagation in tissue to minimize the difference between calculated and optical measurements. This is very similar to the fluorescence molecular imaging problem.[26] Once again, the knowledge of anatomical information will aid the optical reconstruction problem by providing structural detail which may be used to improve optical modeling[27] and reconstruction.[28]

The joint use of x-ray activated phosphors for molecular imaging offers several advantages to x-ray imaging and to all-optical fluorescent imaging. For x-ray imaging, contrast agent imaging is currently limited to high concentrations of nonspecific iodine or barium sulfate. Optimal concentrations for these contrasts have been reported around 300–500 mg/ml.[29] These high concentrations are impractical for imaging biological targets.[2] The ability to image cellular targets would be a great benefit to x-ray imaging, which, despite being the most prominent modality in use in the clinic today, is generally limited to imaging structural anatomy. The use of phosphors combined with the sensitivity of optical imag-

ing allows lower, more biologically feasible concentrations of contrast agents than is currently available with x-ray imaging alone.

The use of x-ray activated phosphors offers three unique advantages to all-optical approaches. First, this dual-modality instrument offers inherent spatial coregistration between anatomical features and optical contrasts. This registration is critical for imaging functional pathology in deep tissue [hence, the need for positron emission tomography (PET)/CT imaging systems].[30] Next, the use of x-ray excitation eliminates the optical autofluorescence issue in optical imaging. Since the x-ray excitation spectrum is undetectable with photo-optical detectors, autofluorescence is avoided, which potentially reduces the detection limit for low concentrations. Finally, this technique is also expected to have increased depth performance over optical imaging, because of the high penetration of x-ray photons in tissues. X-ray photons have nearly two orders of magnitude lower effective attenuation coefficient compared to optical photons; this opportunity offers the potential to use clinically available instrumentation as an external source.

V. CONCLUSIONS

This study focused on the instrumentation and material feasibility of inorganic downconversion phosphors toward the realization of x-ray molecular imaging. Significant recent advances in PET,[4] optical imaging,[11] magnetic resonance imaging,[12] and to a lesser extent, single positron emission computed tomography, and ultrasound have invigorated the search for disease-specific protein receptors that may be targeted with imaging agents. This approach has already been applied to numerous pathologies to identify atherosclerosis and thrombosis,[31] to determine treatment efficacy via apoptosis markers,[32] to identify cancer, and to monitor cellular activity. The incorporation of these markers into x-ray imaging may have significant impact on medical imaging.

In this work, we demonstrate, for the first time to our knowledge, the feasibility of using inorganic phosphors to enable optical detection under x-ray irradiation, which may enable x-ray molecular imaging. We first investigated the practical feasibility of operating a CCD within an x-ray excitation field at clinically relevant energies, taking into consideration noise and potential damage. We found that the dose distribution to air was sufficiently low to prevent damage during operation. Additionally, the noise on the CCD due to incoming high-energy irradiation is manageable. We demonstrated the ability of several phosphors to emit light in the optical regime under x-ray excitation. These phosphors should be effective for tuning light output to a specific application. We found that the light output was linearly proportional to both dose and concentration. Future work will focus on quantitative imaging. We calculated minimum detectable concentrations based on these data and values found in literature; these concentrations are sufficient for certain biological imaging applications. Finally, we demonstrated the potential of inorganic phosphors to image lower concentrations than is possible with x ray alone. We found a 430-fold improvement in contrast recovery for optical detection compared to fluoroscopic detection. This improvement is expected to be greater with modeling of photon propagation and imaging. We envision hybrid x-ray/optical imaging may have significant application in the detection and diagnosis of disease, especially during image-guided intervention.

ACKNOWLEDGMENTS

The authors would like to thank Dr. Catherine Klifa from the University of California, San Francisco for the use of the diffuse optical spectroscopy system. They gratefully acknowledge funding sources from the NSF (Grant No. 0854492), NIH (Grant No. R01 CA133474), and NCI ICMIC (Grant No. P50 CA114747).

[a]Electronic mail: colincarpenter@stanford.edu

[1]F. A. Jaffer and R. Weissleder, "Molecular imaging in the clinical arena," JAMA, J. Am. Med. Assoc. **293**(7), 855–862 (2005).
[2]U. Speck, "Contrast agents: X-ray contrast agents and molecular imaging—A contradiction?," Handb Exp Pharmacol **185**, 167–175 (2008).
[3]R. Weissleder and M. J. Pittet, "Imaging in the era of molecular oncology," Nature **452**(7187), 580–589 (2008).
[4]S. S. Gambhir, "Molecular imaging of cancer with positron emission tomography," Nat. Rev. Cancer **2**(9), 683–693 (2002).
[5]J. Bushberg, J. Seibert, E. Leidholdt, and J. Boone, *The Essential Physics of Medical Imaging*, 2nd ed. (Lippincott Williams & Wilkins, Philadelphia, 2002).
[6]W. M. Yen and M. J. Weber, *Inorganic Phosphors: Compositions, Preparation and Optical Properties* (CRC, 2004)
[7]H. Chander, "Development of nanophosphors—A review," Mater. Sci. Eng. R. **49**(5), 113–155 (2005).
[8]I. Kandarakis, D. Cavouras, G. Panayiotakis, T. Agelis, C. Nomicos, and G. Giakoumakis, "X-ray induced luminescence and spatial resolution of La2O2S:Tb phosphor screens," Phys. Med. Biol. **41**(2), 297–307 (1996).
[9]Y. Jiang, Y. Wu, Y. Xie, and Y. Qian, "Synthesis and characterization of nanocrystalline lanthanide oxysulfide via a La(OH)(3) gel solvothermal route," J. Am. Ceram. Soc. **83**(10), 2628–2630 (2000).
[10]D. Cavouras, I. Kandarakis, T. Maris, G. S. Panayiotakis, and C. D. Nomicos, "Assessment of the gain transfer function of phosphors for application in medical imaging radiation detectors," Eur. J. Radiol. **35**(1), 70–77 (2000).
[11]B. W. Pogue and M. S. Patterson, "Review of tissue simulating phantoms for optical spectroscopy, imaging and dosimetry," J. Biomed. Opt. **11**(4), 041102 (2006).
[12]T. Pham, O. Coquoz, J. Fishkin, E. Anderson, and B. Tromberg, "Broad bandwidth frequency domain instrument for quantitative tissue optical spectroscopy," Rev. Sci. Instrum. **71**(6), 2500–2513 (2000).
[13]C. W. E. van Eijk, "Radiation detector developments in medical applications: Inorganic scintillators in positron emission tomography," Radiat. Prot. Dosim. **129**(1–3), 13–21 (2008).
[14]W. Chen and J. Zhang, "Using nanoparticles to enable simultaneous radiation and photodynamic therapies for cancer treatment," J. Nanosci. Nanotechnol. **6**(4), 1159–1166 (2006).
[15]J. A. Parrish, "New concepts in therapeutic photomedicine: Photochemistry, optical targeting and the therapeutic window," J. Invest. Dermatol. **77**(1), 45–50 (1981).
[16]J. Pickel, A. Kalma, G. Hopkinson, and C. Marshall, "Radiation effects on photonic imagers—A historical perspective," IEEE Trans. Nucl. Sci. **50**(3), 671–688 (2003).
[17]D. Neamen, *Semiconductor Physics and Devices* (McGraw-Hill, New York, 2002).
[18]G. Hopkinson, C. Dale, and P. Marshall, "Proton effects in CCDs," IEEE Trans. Nucl. Sci. **43**(2), 614–627 (1996).
[19]C. Marshall and P. Marshall, "CCD radiation effects and test issues for satellite designers," NASA Electronic Parts and Packaging (2003), p. 1053.

[20]D. A. Boas, D. H. Brooks, E. L. Miller, C. A. DiMarzio, M. Kilmer, R. J. Gaudette, and Q. Zhang, "Imaging the body with diffuse optical tomography," IEEE Signal Process. Mag. **18**, 57–75 (2001).
[21]U. Veronesi, G. Gatti, A. Luini, M. Intra, R. Orecchia, P. Borgen, M. Zelefsky, B. McCormick, and V. Sacchini, "Intraoperative radiation therapy for breast cancer: Technical notes," Breast J. **9**(2), 106–112 (2003).
[22]I. Brigger, C. Dubernet, and P. Couvreur, "Nanoparticles in cancer therapy and diagnosis," Adv. Drug Delivery Rev. **54**(5), 631–651 (2002).
[23]J. Shen, L. Sun, and C. Yan, "Luminescent rare earth nanomaterials for bioprobe applications," Dalton Trans. **42**, 5687–5697 (2008).
[24]C. Vinegoni, D. Razansky, S. A. Hilderbrand, F. Shao, V. Ntziachristos, and R. Weissleder, "Transillumination fluorescence imaging in mice using biocompatible upconverting nanoparticles," Opt. Lett. **34**(17), 2566–2568 (2009).
[25]E. S. M. Ali and D. W. O. Rogers, "Benchmarking EGSnrc in the kilovoltage energy range against experimental measurements of charged particle backscatter coefficients," Phys. Med. Biol. **53**(6), 1527–1543 (2008).
[26]S. C. Davis, B. W. Pogue, H. Dehghani, and K. D. Paulsen, "Contrast-detail analysis characterizes diffuse optical fluorescence tomography image reconstruction," J. Biomed. Opt. **10**(5), 050501 (2005).
[27]D. Hyde, R. Schulz, D. Brooks, E. Miller, and V. Ntziachristos, "Performance dependence of hybrid x-ray computed tomography/fluorescence molecular tomography on the optical forward problem," J. Opt. Soc. Am. A Opt. Image Sci. Vis **26**(4), 919–923 (2009).
[28]A. Li, E. L. Miller, M. E. Kilmer, T. J. Brukilaccio, T. Chaves, J. Stott, Q. Zhang, T. Wu, M. Choriton, R. H. Moore, D. B. Kopans, and D. A. Boas, "Tomographic optical breast imaging guided by three-dimensional mammography," Appl. Opt. **42**(25), 5181–5190 (2003).
[29]Z. Szucs-Farkas, F. R. Verdun, G. von Allmen, R. L. Mini, and P. Vock, "Effect of x-ray tube parameters, iodine concentration, and patient size on image quality in pulmonary computed tomography angiography: A chest-phantom-study," Invest. Radiol. **43**(6), 374–381 (2008).
[30]D. W. Townsend, "Multimodality imaging of structure and function," Phys. Med. Biol. **53**(4), R1–R39 (2008).
[31]R. Weissleder and V. Ntziachristos, "Shedding light onto live molecular targets," Nat. Med. **9**(1), 123–128 (2003).
[32]F. G. Blankenberg, "In vivo detection of apoptosis," J. Nucl. Med. **49**, 81S–95S (2008).